Acoustic emission based damage localization in composites structures using Bayesian identification

2017 J. Phys.: Conf. Ser. 842 012081

(http://iopscience.iop.org/1742-6596/842/1/012081)

IOP Conf. Series: Journal of Physics: Conf. Series **842** (2017) 012081 doi:10.1088/1742-6596/842/1/012081

Acoustic emission based damage localization in composites structures using Bayesian identification

A Kundu[1], M J Eaton[1], S Al-Jumali[2], S Sikdar[3] and R Pullin[1]

[1] Cardiff School of Engineering, Cardiff University, The Parade, Queen's Building, Cardiff, CF24 3AA, UK.
[2] Materials department, College of Engineering, University of Basrah, Basrah, Iraq.
[3] Institute of Fluid-Flow Machinery, Polish Academy of Sciences, 14, Fiszera Street, Gdansk 80-231, Poland.

E-mail: KunduA2@cardiff.ac.uk

Abstract. Acoustic emission based damage detection in composite structures is based on detection of ultra high frequency packets of acoustic waves emitted from damage sources (such as fibre breakage, fatigue fracture, amongst others) with a network of distributed sensors. This non-destructive monitoring scheme requires solving an inverse problem where the measured signals are linked back to the location of the source. This in turn enables rapid deployment of mitigative measures. The presence of significant amount of uncertainty associated with the operating conditions and measurements makes the problem of damage identification quite challenging. The uncertainties stem from the fact that the measured signals are affected by the irregular geometries, manufacturing imprecision, imperfect boundary conditions, existing damages/structural degradation, amongst others. This work aims to tackle these uncertainties within a framework of automated probabilistic damage detection. The method trains a probabilistic model of the parametrized input and output model of the acoustic emission system with experimental data to give probabilistic descriptors of damage locations. A response surface modelling the acoustic emission as a function of parametrized damage signals collected from sensors would be calibrated with a training dataset using Bayesian inference. This is used to deduce damage locations in the online monitoring phase. During online monitoring, the spatially correlated time data is utilized in conjunction with the calibrated acoustic emissions model to infer the probabilistic description of the acoustic emission source within a hierarchical Bayesian inference framework. The methodology is tested on a composite structure consisting of carbon fibre panel with stiffeners and damage source behaviour has been experimentally simulated using standard H-N sources. The methodology presented in this study would be applicable in the current form to structural damage detection under varying operational loads and would be investigated in future studies.

1. Introduction

Maintenance costs for high value assets, such as aircraft and wind turbines, make a significant contribution to operating costs and the successful implementation of structural health monitoring (SHM) systems has the potential reduce these costs by a considerable amount (up to 30M p.a., Airbus sources). Some SHM technologies that have shown good potential in lab scale demonstrations have struggled to translate this performance in to industrial applications because the increseasd structural complexity, noise levels and vatiation in operating conditions leads to increasing uncertainty and lower accuracy. The acoustic emission (AE) technique is one

such approach that has been shown to perform poorly in industrial environments [1]. Despite this poor performance the AE technique has a number of desirable attributes that make it appealling for SHM applications, in particular: it is able to monitor in real-time (making it suitable for in-service monitoring), it is able to globally monitor a structure using a distributed array of sensors and it is possible to both locate and characterise damage. This list of desirable attributes means that addressing the poor performance observed in industrial environments is seen as a worthwhile activity.

Acoustic emission is the phenomenon whereby small amounts of elastic energy are released by changes whithin a material or structure. These changes result from mechanical mechanisms such as crack growth and plastic deformation as well as friction and rubbing (which are often considered noise sources). The energy is released from it point of origin (often referred to as the source) and propagates out in all directions as an elastic stress wave, akin to an ultrasond wave. As with ultrasound waves the elastic stress waves produce minute surface displacements when they arrive at or travel along a surface. These surface displacements can then be converted to a voltage response using a piezoelectric transducer. These transient signals are analysed in real time by most modern AE systems but can also be digitised and stored to allow further signal processing and analysis. If a distributed array of sensors is used to detect the energy released from a single source, or energy release, then triangulation techniques can be utilised to predict the location of the source (i.e. the damage location), in a similar fashion to determining the epicentre of an earthquake in seismology. Figure 1 presents a schematic of the AE measurement process

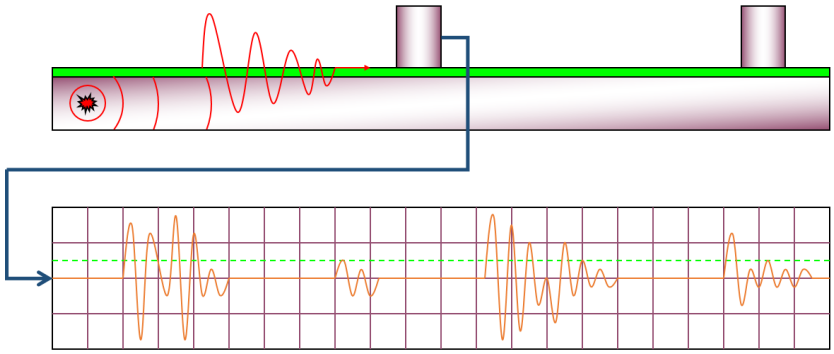

Figure 1. Schematic of AE measurement process.

and it is clear that any changes in the material and/or geometry will affect the resultant recorded signal. Accounting for the boundary uncertainty explicitly in the mathematical model of the physical process is complex and associated with significant computational overhead [2]. Thus accurate damage location using AE in complex structures presents significant challenge. The loss in accuracy observed in complex structures occurs for two specific reasons: firstly a failure to accurately determine the signal arrival time and secondly an overly simplified representation of the AE wave propagation path and velocity in the location calculations [3, 4].

This study aims to overcome the above limitations using a novel approach which trains and calibrates the damage model using a compound correlation metric between the signals recorded with the distributed sensory network. When only using the arrival time of the signal at the individual sensors (and the difference in arrival time) as the basis of training the model, a large portion of the the signal data is not being utilized fully. Additionally error is incurred in the adhoc definitions of signal threshold values which are used to calculate arrival time. Moreover, it is strongly based on the assumption of the existence of a travel path between the damage and the sensor location (this can be considered as an underlying regularization) which might often

not be the case. The proposed methodology, in contrast, constructs a compressed representation of the full signal characteristics using a projected correlation metric (as discussed in section 3) which utilizes the full signal characteristics to infer the source of the incoming waves. The gaussian process based surrogate regression approach explicitly accounts for the uncertainty in lack of training data and/or the error incurred using the process described in section 4.

2. Acoustic emission source location

The traditional approach to determination of the arrival time of an AE signal, and that used in all commercially available systems, is a simple threshold approach whereby a user defined threshold level is set and data is recorded when the transducer voltage response exeeds this level with the first threshold crossing time taken as the signals arrival time. It is, however, possible for signal to be present prior to the first threshold crossing and attenuation of signal amplitude can mean variation in signal arrival time determination. A wide range of approaches have been developed in an attempt to improve the arrival time determination compared with the traditional threshold crossing technique. A range of frequency based techniques including filtering [5], cross-correlation [**?**] and wavelet transforms [6, 7] have been investigated, however, statistical approaches based on 6th order statistical moments [8] and the Akaike Infomation Criteria (AIC) [9, 10] have been shown to be more reliable. The AIC approach in particular has been demonstrates to be very robust across a range of materials and structures [11].

Standard AE location algorithms assume a single, constant, wave propagation speed, however, in composite materials the wave speed is seen to vary with propagation direction and is dependent on fibre orientations within the layup used. Several researchers have tried to address this challenge and some success has been by extending the traditional time of arrival optimization scheme to include a variable wave speed dependent on propagation direction [12, 13]. Ciampa and Meo [14] adopted a novel approach whereby closely spaced sensor pairs were used to reduce the number of unknown propagation velocities in a set of simultaneous non-linear equations that describe the source position. An iterative Newton appraoch was adopted to solve the unknowns in the equations and therefore yield an estimate of the source position without prior knowledge of the wave speeds in the material. Despite these advances achieved in anisotropic monolithic materials, none of the approaches are capable of accounting for geometric complixities such as access holes, curvatures and thickness changes that commonly occur in industrial structures. Alternatively a mapping approach has been proposed and rigorously validated [15, 16, 11, 17, 18] in which a structure is mapped using artificial AE sources (such as a H-N source [19, 20]) to derive an emprical relationship between the known source position and the resultant arrival times at an array of sensors. This relationship can then be used to determine the source origin for a set of measured arrival times. The empirical nature of the approach inherantly accounts for all material and structural complexity such as anisotropy and geometric features.

The previously discussed approaches are deterministic and do not consider the uncertainty in the measurements and calculations performed. This is particularly relevant to their application to industrial environments where uncertainty is seen to increase, with varying operating conditions such as temperature affecting wave propagation and therefore reducing reliability. To account for the uncertainty that can be expereinced in an industrial environment researchers have begun to adopt probabilistic approaches. Schumacher et al [21] developed an approach based on Bayesian statistics for AE source location in a reinforced concrete beams that accounts for uncertainties and errors that exist within the measurement and calculation process. A simplified model for the concrete beam was developed, in which the mean of the wave slowness, the standard deviation of the wave slowness, the event time and the standard deviation of the observed arrival times are represented as prior probability density functions (PDF). The initial PDF of each parameter was then refined using experimental data collected from H-N sources at known positions on the beam surface. The refined model could then be used to predict the

most likely position of any subsequent AE sources. The approach reduced the mean error of 22 arbitrarily located H-N sources from 40mm down to 30mm. Further work by Zarate et al [22] developed a Bayesian framework based on a ray tracing model of AE wave propagation in liquid filled storage tanks. The approach allowed structure bourne and water bourne wave paths to be considered. Using a Markov Chain Monte Carlo (MCMC) method to sample the posterior distribution of the source position in x and y coordinates the most probably source position could be determined. Both of these probabilistic approaches are limited to homogeneous materials and simple geometries, i.e. direct and uninterrupted wave paths.

This main aim to the present work is to combine the Bayesian probabilistic mapping of the source of AE to the correlation characteristics of the signal collected at the distributed sensor network. This would not only capture the essential information pertaining to the phase difference and attenuation of elastic waves travelling different distances over the surface of the composite structures to reach individual sensors but also include the complex effects of boundary reflection within the signal correlation characteristics. The uncertainty due to the measurement noise and experimental errors would be explicitly accounted for in the probabilistic model and conditioned on the training data generated with H-N sources.

3. Important signal characteristics for damage identification

The notion of correlation between the signals observed at different locations in a distributed sensory network is of prime importance in the inference of underlying parameters representative of the physical process. If we consider n_s sensors distributed on the structure under study, the collected signal is represented as

$$\mathbf{X} = \{\mathbf{x}_i : \mathbf{x}_i = [x_i[1], x_i[2], \ldots, x_i[n]]^\intercal \quad \forall i = 1, \ldots, n_s\} \tag{1}$$

where each sample $x_i[j]$ has been collected at sensor i at n discrete time points $j = 1, ldots, n$. An initiation of crack or a growth in crack size is accompanied by a packet of ultrasonic wave which propagates radially outwards from its point of origin along the plane of the composite structure. Each sensor captures signal $x_i[n]$ as show in figure 2. Additionally reflection from

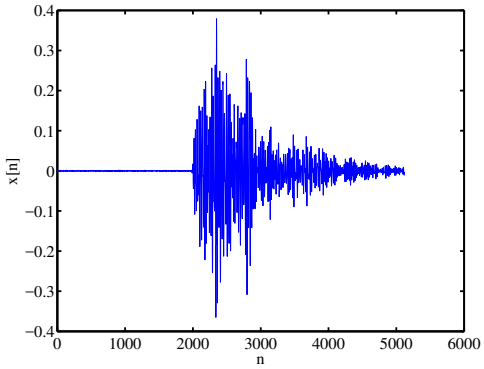

Figure 2. Sample AE signal captured at a particular sensor location.

boundaries and/or other geometrical discontinuities (such as holes) result in a complicated propagation characteristics. It is expected that the accumulated data from the distributed sensory network would contain distinguishing features (statistics) which would map the detected waveforms uniquely to the source location.

The correlation matrix $\bar{\mathbf{R}}$ between the signals collected at each of the n_s sensors is defined as

$$\bar{\mathbf{R}}_\tau = \begin{bmatrix} \mathbf{R}_{11}(\tau) & \mathbf{R}_{12}(\tau) & \cdots & \mathbf{R}_{1n_s}(\tau) \\ \mathbf{R}_{21}(\tau) & \mathbf{R}_{22}(\tau) & & \mathbf{R}_{2n_s}(\tau) \\ \vdots & & \ddots & \vdots \\ \mathbf{R}_{n_s1}(\tau) & \mathbf{R}_{n_s2}(\tau) & \cdots & \mathbf{R}_{n_sn_s}(\tau) \end{bmatrix} \quad 2$$

where each element $\mathbf{R}_{ij}(\tau)$ of the correlation matrix is defined in the continuous time domain as

$$R_{ij}(\tau) = \int_{-\infty}^{\infty} x_i(t)x_j(t+\tau)dt \quad 3$$

for real-valued signal components. For L^1 integrable signals, i.e. $\int_{-\infty}^{\infty} |x(t)|\, dt < \infty$ the Fourier transform of the signal exists and is related to the terms in $\bar{\mathbf{R}}$ matrix. In equation 3, when $i = j$, the terms $\mathbf{R}_{ii}$, i.e. the diagonal terms in the matrix $\bar{\mathbf{R}}_\tau$, give the autocorrelation measure of the signals at each sensor.

For discrete time signals the cross-correlation for real-valued signals is defined as

$$\mathbf{R}_{ij}(\tau) = \mathbb{E}\left[(\mathbf{x}_i[n] - \boldsymbol{\mu}_i)(\mathbf{x}_j[n+\tau] - \boldsymbol{\mu}_j)\right] \quad \forall i, j = 1, \ldots, n_s \quad 4$$

The cross-correlation is often normalized by the respective auto-correlation functions at zero lag such that

$$\mathbf{r}_{ij}(\tau) = \frac{\mathbf{R}_{ij}(\tau)}{\sqrt{\mathbf{R}_{ii}(0)\mathbf{R}_{jj}(0)}} \quad \text{where} \quad |\mathbf{r}_{ij}(\tau)| \leq 1 \quad \forall i, j, \tau \quad 5$$

and we denote the normalized version of $\bar{\mathbf{R}}_\tau$ as $\bar{\mathbf{r}}_\tau$ where each element of the matrix in equation 2 is normalized as per equation 5. It is important to note that $\mathbf{R}_{ij}(\tau) = \mathbf{R}_{ji}(-\tau)$ and $\mathbf{R}_{ij}(\tau) = \mathbf{R}_{ij}(-\tau)$, hence $\mathbf{r}_\tau$ is a symmetric matrix for all τ. The normalized correlation coefficient is utilized here to balancethe varying intensity of the AE source. The mapping which links training dataset to the source location assumes that the source intensity is normalized across the entire training dataset which is achieved with the normalized correlation coefficient.

The power spectral density $\mathcal{S}$ which gives the frequency content of the signal is related to the cross-correlation function by the Fourier transform dual, following Wiener-Khintchin theorem [23], as

$$\mathcal{S}_{ij}(\omega) = \int_{-\infty}^{\infty} R_{ij}(\tau)e^{-i\omega\tau}d\tau \quad \text{and} \quad R_{ij}(\tau) = \frac{1}{2\pi}\int_{-\infty}^{\infty} \mathcal{S}_{ij}(\omega)e^{-i\omega\tau}d\omega \quad 6$$

and when considering windowed signals over finite duration T, the and for discrete time signals it is of the form

$$\mathcal{S}_{ij}(\omega) = \lim_{T\to\infty} \mathbb{E}\left[\frac{1}{T}\ \widetilde{\mathbf{x}}_i^*(\omega)\widetilde{\mathbf{x}}_j(\omega)\right] \quad 7$$

where $\widetilde{\mathbf{x}}_i^*(\omega)$ is the Fourier transform of the time signal $\mathbf{x}_i[n]$. The power spectral density $\mathcal{S}_{ii}(\omega) = \lim_{T\to\infty} \mathbb{E}\left[\frac{1}{T}\ |\widetilde{\mathbf{x}}_i^*(\omega)|^2\right]$ is a measure of the signal's energy distribution over the frequency range. Thus each term of the correlation matrix $\bar{\mathbf{R}}_\tau$ has a spectral decomposition in terms of the power spectral density and are sometimes referred to as integrated spectrum.

The correlation matrix captures the essential information regarding the correlation of the signals captured using the distributed sensor network which contains essential information regarding the delay or phase of the arriving signals. The matrix $\bar{\mathbf{R}}_\tau$ is constructed over the interval $-\tau_s \leq \tau \leq \tau_s$ such that each of its elements $\mathbf{R}_{ij}(\tau)$ or the normalized cross-correlation $\mathbf{r}_{ij}(\tau)$ is a vector of dimension $2\tau_s + 1$. Since the correlation matrix is symmetric, only the upper triangular part is considered in a matrix representation

$$\bar{\mathbf{r}}_{\Delta_k,\tau_s} = \left[\mathbf{r}_{\tau_s,i} : \mathbf{r}_{\tau_s,i} \in \mathbb{R}^{2\tau_s+1} \ \text{ and } \ -\tau_s \leq \tau \leq \tau_s \quad \forall i \in \mathcal{I}\right] \quad 8$$

where $\mathcal{I}$ is the set of indices associated with the ordering of the elements of the upper triangle of $\mathbf{r}_\tau$ at some instance τ and $\mathbf{r}_{\tau_s,i}$ is a vector which contains the cross-correlation measure over the interval $\pm\tau_s$. It is important to note that the subscript Δ_k of the matrix $\bar{\mathbf{r}}_{\Delta_k,\tau_s}$ $k = 1,\ldots,n_t$ denotes normalized correlation data evaluated for the k-th test point out of a total of n_t training sets. Thus the full set of training correlation data is given as

$$\bar{\mathbf{r}}_{\Delta,\tau_s} = \left[\bar{\mathbf{r}}_{\Delta_1,\tau_s}, \bar{\mathbf{r}}_{\Delta_2,\tau_s}, \ldots, \bar{\mathbf{r}}_{\Delta_{n_t},\tau_s}\right] \quad \text{where} \quad \bar{\mathbf{r}}_{\Delta_k,\tau_s} \in \mathbb{R}^{2\tau_s+1 \times n_\mathcal{I}}, \quad k = 1,\ldots,n_t \tag{9}$$

where $n_\mathcal{I}$ is the cardinality of the set $\mathcal{I}$.

The objective here is to obtain a map between the normalized correlation matrix representing the signal data for each of the n_t training sets and the corresponding coordinates of the acoustic source. However, the computational demands of modelling the large predictor matrix $\bar{\mathbf{r}}_{\Delta,\tau_s}$ is substantial and would make the subsequent real-time model prediction infeasible. Thus we seek an optimal reduced basis which can be used to represent the data for each training set such that

$$\begin{aligned} \text{find} \quad & \mathcal{T} : \mathbb{R}^{2\tau_s+1 \times n_\mathcal{I} n_t} \to \mathbb{R}^{n_r \times n_\mathcal{I} n_t} \quad \text{where} \quad \mathcal{T}(\bar{\mathbf{r}}_{\Delta_i,\tau_s}) = \boldsymbol{\alpha}_{i,\tau_s} \quad \forall i = 1,\ldots,n_\mathcal{I} n_t \\ & \text{such that} \quad \Phi_{\Delta,\tau_s} = \underset{\phi_{\Delta_j,\tau_s},\forall j}{\arg\inf} \left\| \Phi_{\Delta,\tau_s}[\boldsymbol{\alpha}_{1,\tau_s},\ldots,\boldsymbol{\alpha}_{n_\mathcal{I} n_t,\tau_s}] - \bar{\mathbf{r}}_{\Delta_i,\tau_s} \right\|_F \end{aligned} \tag{10}$$

where $n_r << 2\tau_s + 1$ and $\boldsymbol{\alpha}_{i,\tau_s} \in \mathbb{R}^{n_r}$. Thus the transformation $\mathcal{T}$ expresses the normalized correlation terms using an optimal basis on which the solution would be projected and an additional orthonormality constraint of $\Phi^\intercal_{\Delta,\tau_s}\Phi_{\Delta,\tau_s} = \mathbf{I}$ can be imposed on the basis. This optimal basis can be informed by the left singular eigenvectors of the training correlation data contained in $\bar{\mathbf{r}}_{\Delta,\tau_s}$ or the principal eigenvectors associated with $\bar{\mathbf{r}}^\intercal_{\Delta,\tau_s}\bar{\mathbf{r}}_{\Delta,\tau_s}$. The compressed correlation data is be expressed in terms of this optimal basis as

$$\underline{\boldsymbol{\alpha}}_{\tau_s} = \{\underline{\boldsymbol{\alpha}}_{1,\tau_s},\ldots,\underline{\boldsymbol{\alpha}}_{n_t,\tau_s}\} = \Phi_{\Delta,\tau_s} \quad \text{where} \quad \bar{\mathbf{r}}^\intercal_{\Delta,\tau_s} \quad \text{where} \quad \underline{\boldsymbol{\alpha}}_{\tau_s} \in \mathbb{R}^{n_r \times n_\mathcal{I} n_t} \tag{11}$$

The matrix $\underline{\boldsymbol{\alpha}}_{\tau_s}$ consists of a collection of $n_\mathcal{I} n_t$ vectors each of dimension n_r, thus for each of the n_t training points we get a set of $n_\mathcal{I}$ vectors which contains the compressed information.

Next we introduce the linear map $vec(\cdot) : \mathbb{R}^{n\times k} \to \mathbb{R}^{nk}$ which transforms a collection of k vectors each of dimension n into a single vectors of dimension nk (where each of the k vectors are stacked end to end). The matrix $\bar{\mathbf{r}}_{\Delta,\tau_s}$ is transformed as

$$\underline{\boldsymbol{\alpha}}_v = \left\{vec(\underline{\boldsymbol{\alpha}}_{1,\tau_s}),\ldots,vec(\underline{\boldsymbol{\alpha}}_{n_t,\tau_s})\right\} \quad \text{where} \quad \underline{\boldsymbol{\alpha}}_v \in \mathbb{R}^{n_r n_\mathcal{I} \times n_t} \tag{12}$$

such that each of the $n_r n_\mathcal{I}$ vector in $\underline{\boldsymbol{\alpha}}_v$ corresponds to the compressed data collected at the distributed sensor network on the structural system.

The problem then defined defined in terms of finding the map $\mathcal{G} : \boldsymbol{\alpha}_{v,xy} \to r_{xy}$ where r_{xy} is a vector of the Euclidean distance of AE source from each sensor in the distributed sensory network and the subscript (xy) denotes the Cartesian coordinates of the AE soruce. The problem is posed as the following multivariate least square regression problem

$$\boldsymbol{\gamma} = \underset{\boldsymbol{\gamma}\in\mathbb{R}^{n_r n_\mathcal{I}}}{\arg\inf} \left\|\boldsymbol{\alpha}_{v,xy}\boldsymbol{\gamma} - r_{xy}\right\|_2 \tag{13}$$

However, for each training run, there is an uncertainty around the measured signal. We construct a scalar error indicator following from equation 13 as

$$\varepsilon_r = \left\|\hat{r}_{xy} - r_{xy}\right\| \quad \text{where} \quad \hat{r}_{xy} = \boldsymbol{\alpha}_{v,xy}\boldsymbol{\gamma} \tag{14}$$

where $\hat{r}_{xy}$ is the approximate identified location of the acoustic source associated with the training data where the known true source is at r_xy distance from the sensors. Equation 14 gives the error associated with the regression map $\mathcal{G} : \boldsymbol{\alpha}_{v,xy} \to r_{xy}$. Thus the error indicator ε_r for the training dataset is mapped on the spatial domain using a Gaussian process surrogate, discussed in the following section, based on which the probabilistic prediction of the source location is performed based on the observed signal data at the distributed sensory network.

4. Bayesian emulation of the error surface

In the previous section, the error indicator ε_r is a function of (x, y) coordinates of the AE source such that $\varepsilon_r : (x, y) \to \mathbb{R}$. In this section, we introduce a Gaussian process model [24] compute a surrogate response surface of the error indicator over the spatial domain of the structural system.

The coordinates (x, y) of the AE source over the domain $[l_x, l_y]$ serves as the parameter space or the input space over which the error indicator ε_r is trained. Here it is assumed that the observed error output vector $[\varepsilon_{r_1}(x, y), \ldots, \varepsilon_{r_{n_t}}(x, y)]$ are realisations of a Gaussian stochastic process with parametrized mean and covariance functions. The model structure is thus expressed as

$$\varepsilon_r(x, y) = \mathbf{h}(x, y)^\intercal \boldsymbol{\beta} + Z(x, y) \tag{15}$$

where $\mathbf{h}(x, y)$ is a vector of known functions and $\boldsymbol{\beta}$ is an unknown hyperparameter to be estimated from the data. The choice of $\mathbf{h}(\boldsymbol{\xi})$ is an active research area [25, 26]. The function $Z(\cdot)$ is a stochastic process with mean zero and covariance function

$$Cov(Z((x, y)), Z(x', y')) = \sigma_z^2 C((x, y), (x', y')) \tag{16}$$

where $C(\cdot, \cdot)$ is a correlation function and σ_z^2 is the process variance, a hyperparameter that can also be estimated from the data. In order to choose a valid positive-definite correlation function, we consider products of one-dimensional correlations[27] with functional forms

$$C((x, y), (x', y')) = \exp\Big\{ - b_i \Big| x - x' \Big|^2 - b_i \Big| y - y' \Big|^2 \Big\} \tag{17}$$

where $b_i > 0$ for all i with $x, x^{'} \in [0, l_x]$ and $y, y^{'} \in [0, l_y]$. The above correlation function is infinitely differentiable which is convenient when Gaussian processes are used to model not only the code output, but also its derivatives [28]. The vector of smoothness hyperparameters $\mathbf{b} = \big(b_1, b_2\big)^\intercal$ quantifies the rate at which the output varies over the spatial domain.

Let $\mathcal{D} = \Big\{ \big((x, y)_i, \varepsilon_r(x, y)_i\big) \Big| i = 1, \ldots, n_t \Big\}$ be a set of n_t training runs. Given this observed dataset, Bayes' theorem is used to estimate the hyperparameters as follows

$$\mathbb{P}(\beta, \boldsymbol{\sigma_z^2}, \mathbf{b} \big| \mathcal{D}) = \frac{\mathbb{P}(\mathcal{D} \big| \beta, \boldsymbol{\sigma_z^2}, \mathbf{b}) \mathbb{P}(\beta, \boldsymbol{\sigma_z^2}, \mathbf{b})}{\mathbb{P}(\mathcal{D})} \tag{18}$$

where $\mathbb{P}(\beta, \boldsymbol{\sigma_z^2}, \mathbf{b} \big| \mathcal{D})$ is the posterior probability of the hyperparameters, $\mathbb{P}(\mathcal{D} \big| \beta, \boldsymbol{\sigma_z^2}, \mathbf{b})$ is the likelihood, $\mathbb{P}(\beta, \boldsymbol{\sigma_z^2}, \mathbf{b})$ is the prior of the hyperparameters, and $\mathbb{P}(\mathcal{D})$ is the marginal likelihood. A detailed derivation of prior-to-posterior analysis along with the hyperparameter estimation is given in [29, 30].

The assumed Gaussian process prior on the code's output implies that the posterior distribution is also a Gaussian process. Once the hyperparameters are estimated, the mean of the posterior distribution approximates the output of ε_r^* at any point (x^*, y^*) on the physical domain. The variance of the posterior distribution quantifies the uncertainty that arises from having only a limited number of observations [31]. It can be shown that the posterior distribution is of the form

$$\varepsilon_r(x, y) \big| \varepsilon^{\text{obs}}, \sigma_z^2 \sim \mathcal{N}\Big(m^*(x, y), \sigma_z^2 C^*((x, y), (x', y')) \Big) \tag{19}$$

where the posterior mean and posterior variance are respectively

$$m^*(x, y) = \widehat{\boldsymbol{\beta}} + \mathbf{r}^\intercal \mathbf{C}^{-1} (\mathbf{y} - \mathbf{1}\widehat{\boldsymbol{\beta}}) \tag{20}$$

$$C^*((x, y), (x', y')) = \mathbf{C}((x, y), (x', y')) - \mathbf{r}^\intercal(x, y) \mathbf{C}^{-1} \mathbf{r}(x, y) \tag{21}$$

In the above expressions, $\mathbf{C} \in \mathbb{R}^{n_t \times n_t}$ such that $[\mathbf{C}]_{ij} = C((x_i, y_i), (x_j, y_j)),\ \forall i, j = 1, \ldots, n_t$, $\mathbf{r}(x, y) \in \mathbb{R}^{n_t}$ such that $\mathbf{r}(x, y) = \big(C((x, y), (x, y)^{(1)}), \ldots, C((x, y), (x, y)^{(n_t)})\big)^\intercal$, and $\mathbf{1} \in \mathbb{R}^n$ such that $\mathbf{1} = \big(1, \ldots, 1\big)^\intercal$.

Finally, it has been shown that if σ_z^2 is integrated out of the posterior distribution, then

$$\frac{\varepsilon(x, y) - m^*(x, y)}{\widehat{\sigma}_z \sqrt{C^*}} \sim t_{n-1} \tag{22}$$

which is a Student's t-distribution with $n-1$ degrees of freedom. Thus, the error indicator can be evaluated at any (x, y) (location predicted by the multivariate least square regression problem in equation 13) and $\varepsilon(x, y)$ gives the uncertainty in the acoustic source location. Once the error response surface surrogate has been trained, the prediction of the error is straightforward and computationally efficient which allows for real-time identification of damage location in the structure under active operating conditions.

The error surface $\varepsilon(x, y)$ trained above is used in conjunction with the least square estimator using correlation characteristics (presented in section 3) to give a probabilistic prediction of the AE source conditional on the training data. At the prediction stage the reduced correlation matrix, constructed using the optimal basis Φ_{Δ,τ_s}, is mapped to the AE source and the associated error is evaluated from the trained Gaussian process surrogate in equation 22. Thus a robust probabilistic estimate of the AE source location is obtained using the correlation characteristics of the signal collected from the distributed sensor network. The above procedure is summarized

Algorithm 1 Source localization with Bayesian identification using sensor cross-correlation

Input: Sensor signal data: $\mathbf{X} = \{\mathbf{x}_i : \mathbf{x}_i = [x_i[1], x_i[2], \ldots, x_i[n]]^\intercal \quad \forall i = 1, \ldots, n_s\}$
Input: Equidistant test grid on plate surface: $\{\vec{r}_i : i = 1, \ldots, n_d\}$
Output: Source location $\vec{r}_s$ and the uncertainty around it $\varepsilon(\vec{r}_s) \sim \pi(\theta|\vec{r}_s)$

for $k = 1$ to n_d **do**
  Accumulate sensor data for grid point k: $\{x_1, \ldots, x_{n_s}\}$ where $x_i \in \mathbb{R}^{n_t}\ \forall i$
  for $i = 1$ to n_s **do**
    for $j = i$ to n_s **do**
      Calculate normalized cross-correlation $(\bar{\mathbf{r}}_{\Delta_k,\tau_s})_{ij} \in \mathbb{R}^{2\tau_s+1}$
    end for
  end for
  Assemble the upper triangular cross-correlation matrix $\bar{\mathbf{r}}_{\Delta_k,\tau_s} \in \mathbb{R}^{2\tau_s+1 \times n_{\mathcal{I}}}$
end for
Compressed representation of $\bar{\mathbf{r}}_{\Delta_k,\tau_s}$ as $\mathcal{T}(\bar{\mathbf{r}}_{\Delta_i,\tau_s}) = \boldsymbol{\alpha}_{i,\tau_s}$ using optimal basis Φ_{Δ,τ_s}.
Solve $\boldsymbol{\gamma} = \arg\inf_{\boldsymbol{\gamma}} \|\boldsymbol{\alpha}_{v,\tau_s}\boldsymbol{\gamma} - \vec{r}\|_2$ which maps $\boldsymbol{\alpha}_{i,\tau_s}$ to $\vec{r}$
Approximation error $\varepsilon_{r_i} = \boldsymbol{\alpha}_{v,\tau_s}\boldsymbol{\gamma} - \vec{r},\ \ \forall i \in n_d$ for each test point on grid
A prior for Gaussian process surrogate: $\varepsilon_{r_i} \sim \mathcal{N}(\mu, Z(\vec{r})|\theta)$ with hyper-parameter set θ.
Obtain posterior: $\varepsilon_r(\vec{r})\big|\varepsilon^{\text{obs}}, \theta^* \sim \mathcal{N}\Big(\mu_\theta^*(\vec{r}), Z_\theta^*(\vec{r})\Big)$ conditioned on training data ε^{obs}
globals Φ_{Δ,τ_s}, μ^*, Z^*, θ^*
Compute $\hat{\mathbf{r}}_{\Delta,\tau_s}$, the normalized cross-correlation with test data
Evaluate: $\boldsymbol{\alpha}_{v,\tau_s} = \hat{\mathbf{r}}_{\Delta,\tau_s}^T \Phi_{\Delta,\tau_s}$ and $\vec{r}\_0 = \boldsymbol{\alpha}_{v,\tau_s}\boldsymbol{\gamma}$
Prediction: $\vec{r}_c = \vec{r}_0 + \mathcal{N}\Big(\mu_\theta^*(\vec{r}_0), Z_\theta^*(\vec{r}_0)\Big)$

in Algorithm 1 whereby the steps to obtain posterior prediction from a probabilistic surrogate has been listed.

5. Experimental setup

In order to develop and validate the above approach for damage localization, data was collected from a stiffened carbon fibre composite panel, representative of an aerospace structure.

5.1. Sample details

The manufactured stiffened panel is presented in Figure figure 3. The stiffeners were purchased from Easy Composites Ltd. (Staffordshire, UK) they consist of a 90^o L-shaped cross-section with laminate thickness of 3mm and cross-section dimensions of 25×25mm and a length of 600mm. The stiffeners are made from 2×2 twill high strength carbon fibres in an epxoy matrix

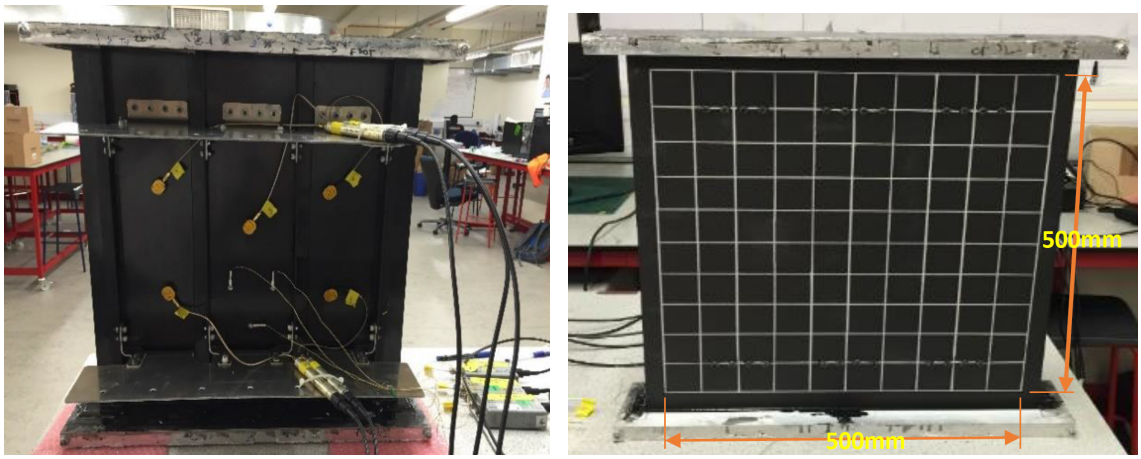

(a) Stiffener side (b) Grid side

Figure 3. Manufactured panel a) from stiffener side showing sensor positions and b) from skin side showing grid used for data collection.

with fibres aligned in the 0^o and 90^o directions. The skin was manufactured from 12 plies of Cytec MTM28/T800HB/200/42% 2×2 twill weave carbon fibre composite material with a $(0)_{12}$ layup and was cured in an autoclave in line with the manufacturers recommended cure cycle. Following curing the thickness was 2.85mm and the skin panel was cut to 550×600mm using a water cooled diamond tipped cutting wheel. The skin and stiffeners were lightly abraded and degreased in preparation for bonding using permabond ET5429 adhesive. The final overall panel dimensions were 550×600mm with the stiffeners running vertically. Two aluminium dumby ribs (representative of attachment to a wing rib for a composite wing skin) were attached at 1/4 and 3/4 hight of the panel by drilling and bolting using 12 M4 bolts for each, as seen in 3(a). The top and bottom edges of the panel were potted into 20mm deep aluminium frames using Airtech TMR2001 high temperature laminating resin to allow application of a compressive load (not considered in this paper). A 500×500mm grid with 50mm resolution was applied to the skin side of the panel (3(b)) and was used to aid the collection of training data.

5.2. Panel instrumentation

The panel was instrumented with eight AE sensors as seen in 3(a), five McWade NS-3303 (300 kHz), the larger gold coloured sensors, and three Mistral Group Ltd. Nano30 sensors (300kHz), the smaller silver sensors. Four McWade sensors are arranged in a 275×175mm square with the fifth placed centrally. The Nano30 sensors are arranged in a 75mm spaced triangular array. The sensor outputs are amplified by 40dB using a McWade PA3303 pre-amplifier for the McWade sensors and a Mistral Group Ltd. 2/4/6 (20-1200kHz) pre-amplifier for the Nano30 sensors. A

silicon adhesive (Loctite 595) was used to attatch the sensors and provide a suitable acoustic couplant, the adhsive was allowed to cure for 24 hrs before any data acquisition or testing was undertaken and the correct coupling of the sensors was assessed using a H-N source [19, 20]. The AE data was recorded with a Mistras Group Ltd. PCI-2 acquisition system using a 45dB threshold level. The detected signals were sampled at 5MHz for a duration of 1000μs: 600μs after the threshold crossing point and with a pre-trigger of 400μs. The time when the threshold crossing occurs for each test point has been recorded and shown in figure 4 and has been discussed in section 6.

5.3. Data acquisition

AE data was collected from the manufactured composite panel using a H-N source [19, 20] to excite artificial AE waves. The H-N source is recognised as a standard reference source (ASTM E976) for AE testing and requires the fracture of a 0.5mm diameter 2H pencil lead agains the sample surface at an angle of 30^o. This is facilitated using a propelling pencil fitted with a plastic rocker the rocker is placed on the sample and the pencil rotated until the lead contacts the surface and then fractures. This results in minute elastic deformation of the surface under the tip of the pencil lead and when the lead fractures the elastic energy stored in the surface is rapidly released and excites a broadband elastic stress wave. This is highly representative of the rapid release of elastic energy that occurs when cracks and fractures grow in materials and hence is why it has been adopted as a standardised reference source for AE testing. The H-N source commonly excites a larger amplitdue signal than a real fracture, however, the source mechanism is still representative and it has been shown to be a suitable artificial source for training a system for the detection and analysis of AE signals from real fracture events as seen in the Delta T Mapping techniques discussed above.

The data used in this work were collected using H-N sources performed at the nodes of the grid applied to the front of the stiffened panel. Ten H-N sources were conducted at each of the grid nodes within the 500×500mm grid shown in 3(b) and for each H-N source eight AE signals were recorded and stored (one from each sensor).

6. Results and discussion

A sample of the collected sensor data is shown in figure 4 where each red dot signify the time (x-axis) of arrival of the wave at a sensor (8 sensors denoted by Ch 1" to "Ch 8") and its maximum amplitude (y-axis). A "hit" is recorded when the signal received at a particular sensor exceeds a preset threshold value. Figure 4 shows the *hits* recorded simultaneously at all the eight sensor locations. All the hits between the vertical blue lines on each channel indicate a test performed with the H-N source at a grid point (figure 3(b)) on the panel. Around 10 tests have been performed at each grid point due to which there are approximately 10 hits (red dots) between two consecutive blue lines. The red dots are aligned in time across all channels except for the small time difference associated with the waves travelling different distances from the source to reach each sensor. All the tests represented in figure 4 have been performed along the 11 test grid points at $x = 0$ (the bottommost line in the grid). This figure essentially represents only the time of arrival for the signal at the individual sensors, but the correlation measure between the sensors is shown in the next figure.

Figure 5 shows the elements of the normalized correlation matrix $\bar{\mathbf{r}}_\tau$ (described in equation 5) where the dimension of $\bar{\mathbf{r}}_\tau$ for a particular τ is 8×8 since we have 8 sensors distributed over the physical domain of the composite structure. Each sub-window in the figure denotes the correlation $\mathbf{r}_{ij}(\tau)$ over $-100 \leq \tau \leq 100$. The figure shows that the autocorrelation function is symmetric, i.e. $\mathbf{r}_{ij}(\tau) = \mathbf{r}_{ij}(-\tau)$ and $\mathbf{r}_{ij}(\tau) = \mathbf{r}_{ji}(tau)$. The correlation function is treated as an energy indicator of the waveforms recorded by each sensor as well as containing essential information about the phase of the waves arriving at each sensor.

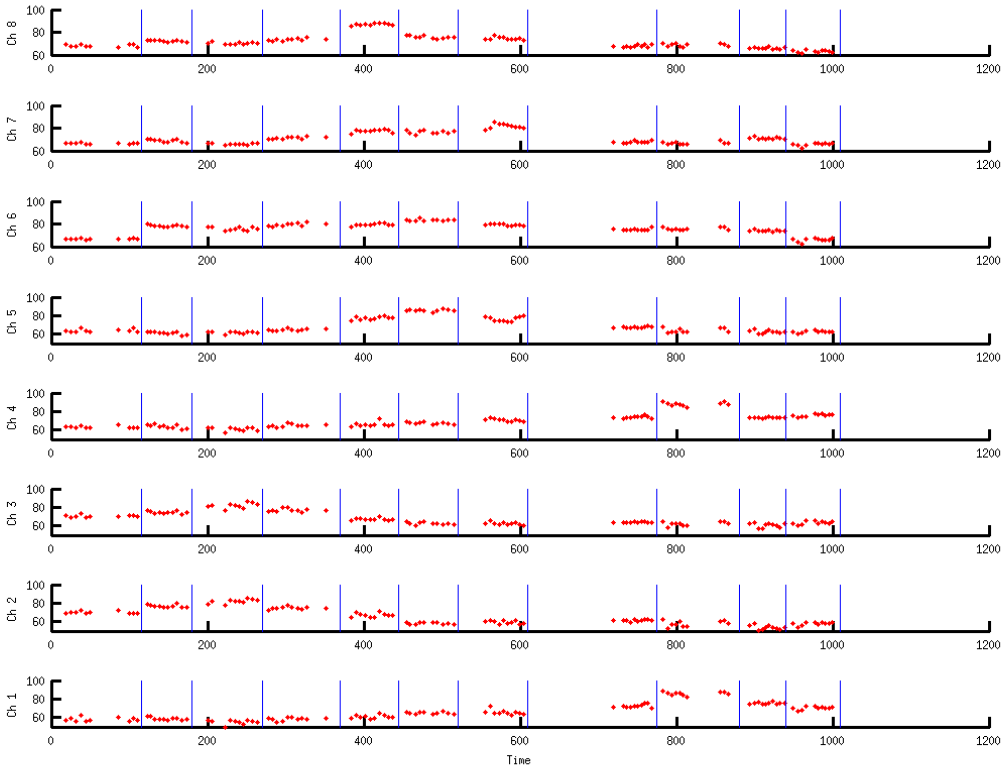

Figure 4. Normalized correlation coefficients of the signal collected at the distributed sensor network (only the first 4 out of the total of 8 sensor signals shown) over discrete time steps $-100 \leq \tau_s \leq 100$

The optimal basis on which the correlation matrix is projected to obtain a compressed representation of the information collected at the sensors is shown in figure 6 A total of 30 basis functions have been used to approximate the terms of the correlation matrix. The basis functions are orthonormalized and have been calculated using the left eigenvectors of the correlation matrix using the singular value decomposition. The rapidly decaying singular value spectrum of the ensures that a good approximation is obtained with the reduced basis. The correlation matrix projected on these 30 optimal bases is termed as the reduced correlation matrix.

The accuracy of the identified AE source using the least square estimate is shown in figure 8. The black dots indicate the training points on the 10×10 grid of the composite panel while the red dots indicate the approximate identified acoustic source locations obtained using the least square mapping of the reduced correlation matrix to the vector of the distance of the acoustic source from the sensor network (as discussed in equation 13). The error $\varepsilon_r(x, y)$ is given by the distance of the identified source locations (red dots) to the known position of AE (black squares).

This error indicator $\varepsilon_r(x, y)$ varies as per the accuracy of the fit and a Gaussian process surrogate is used to build a probabilistic error surface over the spatial domain as discussed in section 4. Figure 8 gives the mean and standard deviation of the posterior error surface conditional on the observations. This gives a distribution of the accuracy of the least sqaures

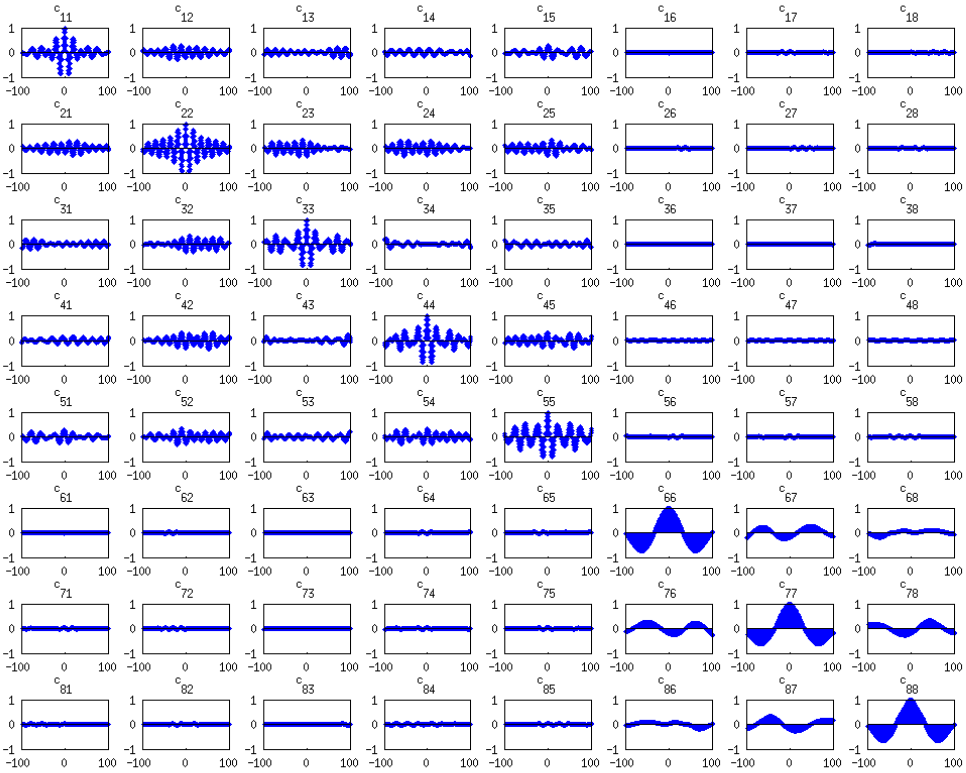

Figure 5. Normalized correlation coefficients of the signal collected at the distributed sensor network over discrete time steps $-100 \leq \tau_s \leq 100$

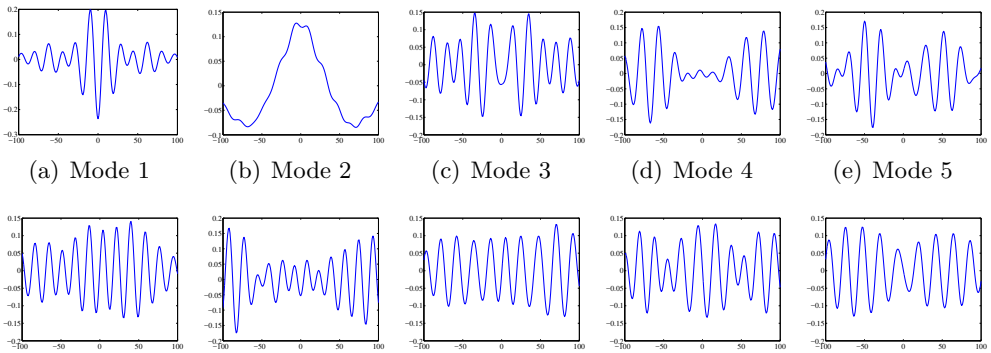

(a) Mode 1 (b) Mode 2 (c) Mode 3 (d) Mode 4 (e) Mode 5

(f) Mode 6 (g) Mode 7 (h) Mode 8 (i) Mode 9 (j) Mode 10

Figure 6. The first 10 modes of the reduced basis for the normalized correlation matrix

estimate as a function of the spatial coordinates. It can be verified that the mean error is almost zero at those training locations where the accuracy of the least square method is maximum. The locations where there are no training points show a high value of mean error and correspondingly high standard deviation of error which is an expected behavior.

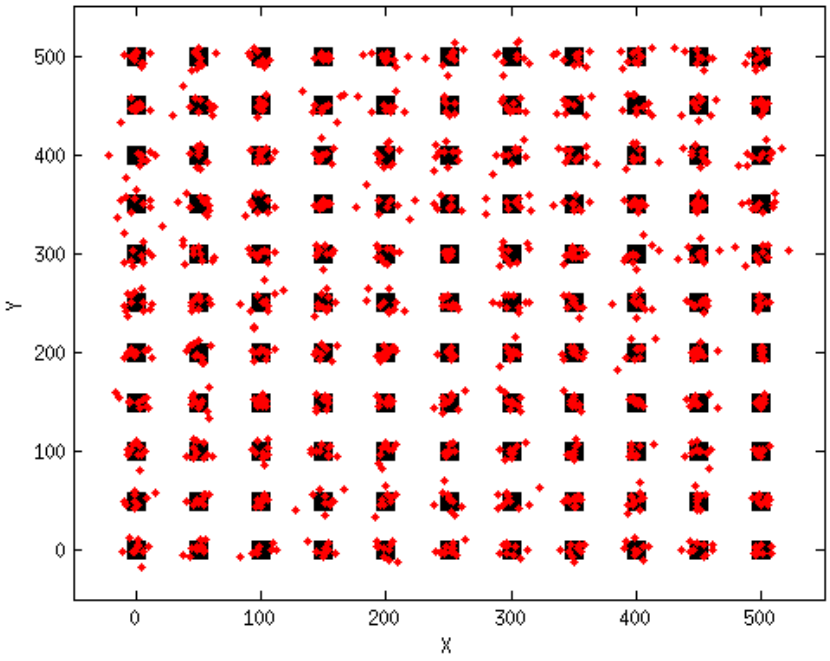

Figure 7. The accuracy of fit of the training dataset based on the observed correlation matrix over the physical domain of the composite panel. The square blocks shown in black constitute the actual test grid while the red dots are least square estimates of the AE source.

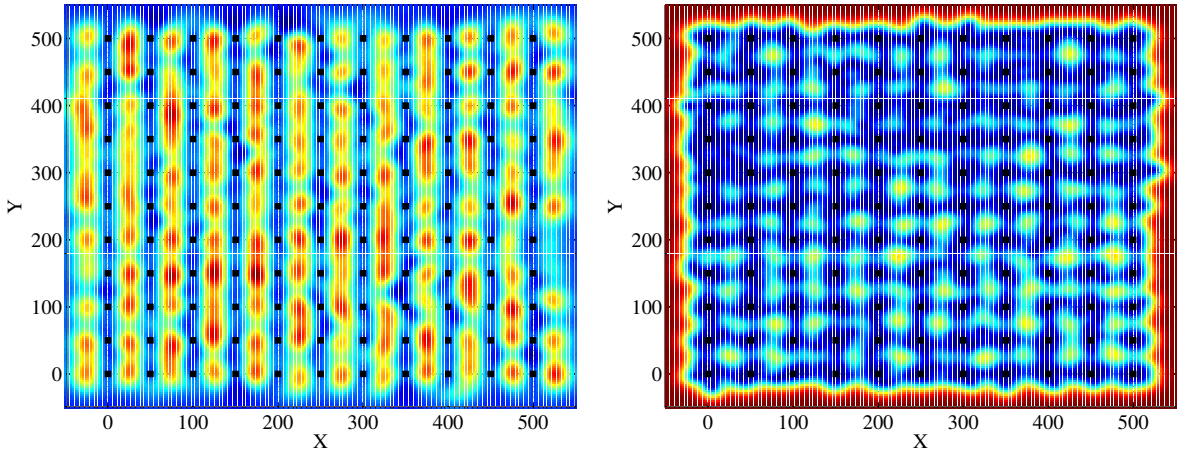

(a) Mean of the error surface (b) Standard deviation of the error surface

Figure 8. The mean an standard deviation of the error response surface over the domain of the plate. The colormap of (a) varies between $0 - 45$mm while for the standard deviation is between $0 - 20$mm

Figure 9 shows the probability distribution associated with an identified test point. The actual location of the acoustic source is shown as the green dot (although this information has not been used to train the model). The assumed gaussian process surrogate predicts the probability distribution of the identified acoustic source location conditional on the training data

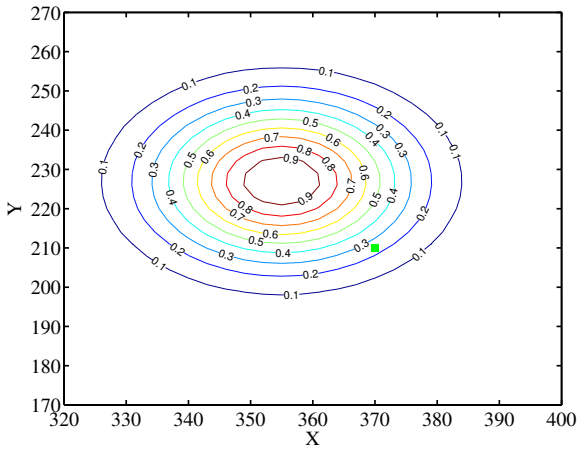

Figure 9. The probability distribution associated with a source identification. The true source is shown as a green dot.

and though the mean true location does not match the exact source location (which is expected due to experimental errors and measurement noise), the true source location is contained within the 95% probability envelope as shown in figure 9.

Thus effectiveness of the methodology is demonstrated in terms of the accuracy of identifying the source of the AE. The cost of producing the gaussian process surrogate is incurred mostly in an offline training stage while in the online identification stage the effective location of the AE source is derived efficiently from the surrogate. This allows for implementation of the technique in real-time identification procedure within the performance constraints of the signal processing platforms.

7. Conclusion and future work

The study demonstrates the effectiveness of the proposed correlation matrix based identification of AE sources in applications of non-destructive testing. The effectiveness of the method stems from using direct evaluations of normalized autocorrelation functions which effectively reduces the impact of signal noise and captures the essential correlation information between the signals recorded with the distributed sensor network. A reduced set of basis vectors which compress the correlation information reduces the memory and computational overhead associated with the method. A Gaussian process surrogate is fitted on the error surface over the spatial domain to explicitly consider the error associated with deterministic evaluators. The results demonstrate the effective of the method in predicting the source location with test data on the same panel.

The study promises a number of interesting future investigations to extend and improve the proposed methodology to address additional challenges. Some of these are

- The application of the proposed methodology to identify the generation cracks on the composite panel under fatigue loading cycles.
- The portability of the trained surrogate i.e. the ability of the trained model to predict AE sources in nominally similar test panels.
- A hierarchical probabilistic model of the AE source mapped to the correlation matrix, where identification stages can be compartmentalized to correspond to various levels of refinement. This would involve the use of a combination of probabilistic classification and regression methodology in an automated sequence to improve the accuracy and minimize the computational overhead associated with the method.

Subsequent work would also focus on using physics based model of ultrasonic wave propagation in composite panels which would provide a means of identifying the nature of damage induced in the structure which has not been addressed in this study. This would allow us to go beyond the black-box input-output mapping techniques which is expected to significantly improve the performance of the identification algorithm and provide additional information pertaining to the degradation of health of operational structures.

Acknowledgments

AK acknowledges the support from Sêr Cymru NRN, Wales through the award of the Industrial Fellowship.

References

[1] Holford K, Eaton M, Hensman J, Pullin R, Evans S, Dervilis N and Worden K 2017 **In press**
[2] Kundu A, Adhikari S and Friswell M I 2014 *International Journal for Numerical Methods in Engineering* **100** 183–221
[3] Miller R, Carlos M, Findlay R, Godinez-Azcuaga V, Rhodes M, Shu F and Wang W 2005 *Acoustic Emission Source Location* (ASNT) pp 121–146 3rd ed
[4] Eaton M, Pullin R and Holford K 2012 *Journal of Mechanical Engineering Science, Proceedings of the Institution of Mechanical Engineers Part C* **226** 2141–2153
[5] Miller R, Anastasopoulos A, Carlos M, Demeski R, Vallen H and Walker J 2005 *Acoustic Emission Signal Processing* (ASNT) pp 147–180 3rd ed
[6] Aljets D, Chong A, Wilcox S and Holford K 2010 *Journal of Acoustic Emission* **28** 85–98
[7] Hamstad M, O'Gallagher A and Gary J 2002 *Journal of Acoustic Emission* **20** 62–82
[8] Lokajicek T and Klima K 2006 *Measurement Science and Technology* **17** 2461–2466
[9] Akaike H 1974 *Annals of the Institute of Statistical Mathematics* **26** 363–387
[10] Kurz J H, Grosse C and Reinhardt H W 2005 *Ultrasonics* **43** 538–546
[11] Pearson M, Eaton M, Featherston C, Pullin R and Holford K 2016 1–18
[12] Kundu T, Das S and Jata K 2007 *Journal of the Acoustical Society of America* **122** 2057–2066
[13] Kundu T, Das S, Martin S and Jata K 2008 *Ultrasonics* **48** 193–201
[14] Ciampa F and Meo M 2010 *Composite Part A* **41** 1777–1786
[15] Baxter M, Pullin R, Holford K and Evans S 2007 *Mechanical Systems and Signal Processing* **21** 1512–1520
[16] Eaton M J, Pullin R and Holford K 2012 *Composites Part A* **43** 856–863
[17] Al-Jumaili S, Pearson M, Holford K, Eaton M and Pullin R 2016 **72-73** 513–524
[18] Scholey J, Wilcox P, Wisnom M and Friswell M 2009 *Ultrasonics* **49** 538–548
[19] Hsu N N and Breckenridge F R 1981 *Materials Evaluation* **39** 60–68
[20] ASTM 2010 *American Society for Testing and Materials,* **E976**
[21] Schumacher T, Straub D and Higgins C 2012 **331**(19)
[22] Zarate B, Pollock A, Momeni S and Ley O 2014 **24**(1)
[23] Chatfield C 2016 *The Analysis of Time Series: An Introduction, Sixth Edition* (CRC Press)
[24] Kundu A, DiazDelaO F, Adhikari S and Friswell M 2014 *Computer Methods in Applied Mechanics and Engineering* **270** 201 – 219
[25] Oakley J E and O'Hagan A 2004 *Journal of the Royal Statistical Society B* **66** 751–769
[26] Keane A and Nair P 2005 *Computational Approaches for Aerospace Design* (Chichester, UK: John Wiley & Sons)
[27] Sacks J, Welch W, Mitchell T and Wynn H 1989 *Statistical Science* **4** 409–435
[28] O'Hagan A 1992 *Bayesian Statistics 4* (Cambridge, UK: Oxford University Press) chap Some Bayesian numerical analysis, pp 345–363
[29] Haylock R and O'Hagan A 1996 *Bayesian Statistics 5* (Oxford, UK: Oxford University Press) chap On inference for outputs of computationally expensive algorithms with uncertainty on the inputs
[30] Oakley J 2002 *The Statistician* **51** 81–97
[31] Rougier J 2007 *Climatic Change* **81** 247–264